

Quantum-enhanced performance in superconducting Andreev reflection engines

Gonzalo Manzano  and Rosa López 

Institute for Cross-Disciplinary Physics and Complex Systems IFISC (UIB-CSIC), E-07122 Palma de Mallorca, Spain



(Received 23 February 2023; revised 4 May 2023; accepted 13 July 2023; published 12 October 2023)

When a quantum dot is attached to a metallic reservoir and a superconducting contact, Andreev processes lead to a finite subgap current at the normal lead and the creation or destruction of Cooper pairs. Andreev reflection engines profit from the destruction of Cooper pairs to provide the work needed to set a charge current at the normal-conductor contact generating electrical power. For this power-transduction device, high power and large efficiencies in quantum mechanically enhanced regimes are demonstrated. Their thermodynamic tradeoff relations between power, efficiency, and stability, valid for any classical engine, are overcome, and kinetic constraints on the engine precision are largely surpassed in arbitrary far-from-equilibrium conditions.

DOI: [10.1103/PhysRevResearch.5.043041](https://doi.org/10.1103/PhysRevResearch.5.043041)

I. INTRODUCTION

At the interface of a normal metal and a superconductor, Andreev reflection allows electron-to-hole conversion by means of the creation of a Cooper pair in the superconductor [1]. The superconducting leakage in the vicinity of a normal metal induces superconducting correlations at the normal side that have a strong impact on the electronics of such systems. Hybrid normal-superconductor (NS) setups have attracted a great deal of interest both from the theoretical [2] and experimental sides [3]. The related phenomena, such as the Josephson effect [4–7] and multiple Andreev reflections [8], are employed as quantum advantages for creating a wide range of possibilities for new electronic devices, including supercurrent transistors [9–11], generators of spin-entangled electrons [12–19], superconducting quantum interference devices [20–25], superconducting single-photon detectors [26], NS-based qubits like Andreev qubits [27–29], and topological qubits [30–32]. The latter have been proposed as building blocks for fault-tolerant quantum computation.

Beyond these applications, hybrid platforms are perfect candidates for thermal machines [33]. In particular, they are being proposed in implementations of quantum refrigerators and heat engines [34–44]. To progress in this field, a comprehensive understanding of their quantum thermodynamics is certainly needed. For such a purpose, we consider a normal conductor acting as a small quantum dot (QD) that is tunnel-coupled to a metallic contact and a superconducting electrode. Quantum dots are attractive for thermodynamics as they can display some quantum advantages, namely, they exhibit quantum level discretization behaving as energy filters, and they can be attached to quantum materials such as reservoirs of coherent states, i.e., Cooper pairs reservoirs.

In this paper, we characterize the quantum performance of a minimal hybrid quantum device based on Andreev reflection processes at the level of its efficiency, power, and its reliability. The device is able to operate in nonequilibrium steady-state conditions as an engine transforming coherent Cooper pairs into an electrical current (see Fig. 1). We dub this device an Andreev reflection engine. Contrary to standard heat engines converting heat into work [45], this engine is an example of a work-to-work converter, a energy transduction mechanism typical in soft nanomachines, working in the presence of various concentration gradients, external forces and torques, or electric fields [46–48]. Here the destruction of Cooper pairs in a quantum dot previously loaded from a superconductor generates an electron-hole pair at the normal contact due to the Andreev processes, i.e., a finite charge current going against the applied bias voltage ($\dot{W}_q > 0$), at the expense of a coherent input power from the superconductor ($\dot{W}_S < 0$). Inversely, because of Andreev processes, a hole can be injected into the normal contact to create a Cooper pair at the superconducting side ($\dot{W}_S > 0$) and a retroreflected electron at the metallic contact ($\dot{W}_q < 0$).

Remarkably, the Andreev reflection engine shows large violations of the so-called thermodynamic uncertainty relation (TUR) and the kinetic uncertainty relation (KUR), which are responsible for the quantum-enhanced performance of the engine operation. The TUR is a universal nonequilibrium relation in the form of an inequality. It imposes strict bounds on the precision of generic currents through a system following classical Markovian evolution in terms of its dissipation as measured by the entropy production rate [49–51]. Relevant applications of the TUR include the estimation of dissipation in systems where only partial information is available [52]. Moreover, the TUR has been used to assess the universal tradeoff between efficiency, power, and their fluctuations in steady-state heat engines, predicting an inevitable drop of stability in any classical engine as their power and efficiency simultaneously increase [53]. As a consequence, violations of the TUR have been proposed as a witness for quantum-thermodynamic signatures in the operation of quantum devices in general [54–56], and quantum heat

Published by the American Physical Society under the terms of the Creative Commons Attribution 4.0 International license. Further distribution of this work must maintain attribution to the author(s) and the published article's title, journal citation, and DOI.

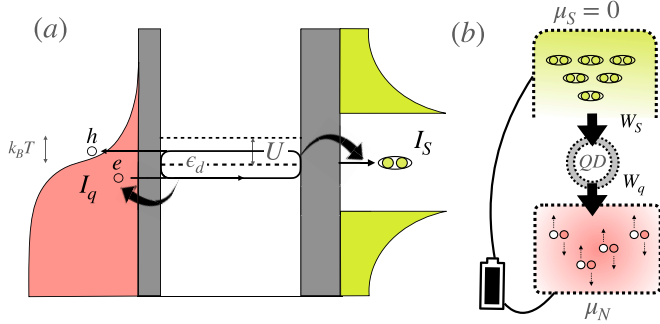


FIG. 1. (a) Illustration of the normal-quantum dot-superconducting engine. In Andreev reflection from the normal metal (left pink terminal) is injected in the quantum dot resulting in (i) a retroreflected hole at the normal reservoir, and (ii) a coherent Cooper pair at the superconductor (right green terminal). (b) The superconductor acts as a source of coherent states (Cooper pairs) that are employed through the quantum dot to generate an electrical current eventually delivering electrical power.

engines in particular [57–62]. However, the relevance of the regimes in which the TUR has been found to break down in previous works is still unclear, given also the small magnitude of the observed violations in many cases. Similar to the TUR, the KUR consists of a universal bound on generic system currents in terms of dynamical activity [63], which, contrary to dissipation, is symmetric under time reversal [64]. Despite passing almost unnoticed, the KUR can provide a powerful complement to the TUR in the description of engines working in nonequilibrium steady states [65], especially in far-from-equilibrium regimes [63,66] where the TUR becomes far from tight [51] (see also Ref. [67] for a unification of TUR and KUR inequalities). Extensions of the original TUR and KUR for quantum dynamics have also been recently reported [68–71]. As we will discuss in the following, Andreev reflection engines are able to show unprecedentedly large violations of the KUR at maximum power, combined with notable violations of the TUR in high-power and high-efficiency regimes. Moreover, both inequalities can be violated simultaneously in a regime with balanced efficiency and close-to-maximum power output.

II. ANDREEV REFLECTION ENGINE MODEL

We consider a single QD device with Hamiltonian $H_d = \sum_{\sigma} \epsilon_{\sigma} d_{\sigma}^{\dagger} d_{\sigma} + U d_{\uparrow}^{\dagger} d_{\downarrow}^{\dagger} d_{\downarrow} d_{\uparrow}$, where ϵ_{σ} denotes the energy level of the dot for electrons with spin $\sigma = \{\uparrow, \downarrow\}$, and U stands for the Coulomb repulsion between electrons. Eventually, one can consider the action of a magnetic field by including a Zeeman splitting in the dot level energy as $\epsilon_{\uparrow, \downarrow} = \epsilon \pm \Delta_Z$ with $\Delta_Z = \mu_B g B$ (μ_B being the Bohr magneton, g is the gyromagnetic factor, and B is the applied magnetic field). The QD is weakly coupled to both a superconducting electrode and to a metallic contact that acts as a thermal reservoir, allowing tunneling of electrons to the QD. Both terminals are kept at a constant temperature T and we assume, without loss of generality, vanishing chemical potential in the superconductor, $\mu_S = 0$. We are interested in the limit of a large superconducting gap, $\Delta \rightarrow \infty$ (subgap transport) [2,72–76], that allows us to approximate the effect of the

superconductor on the dot as a coherent driving, described by an effective time-dependent Hamiltonian reading $H_S(t) = \Gamma_S (d_{\uparrow}^{\dagger} d_{\downarrow}^{\dagger} e^{i(2\epsilon+U)t} + d_{\downarrow} d_{\uparrow} e^{-i(2\epsilon+U)t})$ in a Schrödinger picture. Here Γ_S is a local pairing term that accounts for the proximity effect of the superconductor on the QD. The QD is tunnel-contacted to a normal electrode characterized by the tunneling rate Γ_N . Assuming Born-Markov approximations (either $\Gamma_N \ll |\epsilon - \mu_N|$ or $\Gamma_N \ll k_B T$ [77]) and weak pairing ($\Gamma_S \sim \Gamma_N$), the dynamical evolution of the system can be modeled by a local quantum master equation in Lindblad form describing the driven-dissipative dynamics of the dot (see Appendix A) reading, in the interaction (rotating) frame with respect to H_d ,

$$\dot{\rho}(t) = -i\Gamma_S [d_{\uparrow}^{\dagger} d_{\downarrow}^{\dagger} + d_{\downarrow} d_{\uparrow}, \rho(t)] + \sum_k \mathcal{D}_k[\rho(t)], \quad (1)$$

with dissipators $\mathcal{D}_k[\rho] := L_k \rho L_k^{\dagger} - \frac{1}{2} \{L_k^{\dagger} L_k \rho + \rho L_k^{\dagger} L_k\}$ and a set of eight Lindblad operators labeled as $L_{\sigma, \delta}^{+} = \Gamma_N f(\epsilon_{\sigma} + \delta U) d_{\sigma}^{\dagger}$ and $L_{\sigma, \delta}^{-} = \Gamma_N [1 - f(\epsilon_{\sigma} + \delta U)] d_{\sigma}$, with $\delta = \{0, 1\}$ (and $k = \{\sigma, \delta\}$). These terms describe the incoherent tunneling of electrons from the normal-metal reservoir, jumping inside (+) or outside (−) the dot, at a given energy. Here Γ_N is the tunneling rate between the dot and the normal electrode, and $f(E) = 1/[1 - \exp[(E - \mu_N)/k_B T]]$ is the Fermi-Dirac distribution, with μ_N the chemical potential of the normal-metal reservoir. From the master equation (1), we analytically obtain the density matrix in the steady state $\rho(t \rightarrow \infty) = \pi$ ($\dot{\rho} = 0$) from which we compute the average steady-state energy current $\langle J_E \rangle := \text{Tr}[H_d \sum_k \mathcal{D}[L_k](\pi)]$ and charge current $\langle J_q \rangle := e \sum_{\sigma} \text{Tr}[d_{\sigma}^{\dagger} d_{\sigma} \sum_k \mathcal{D}[L_k](\pi)]$ entering the dot from the normal-metal reservoir. They read

$$\langle J_E \rangle = \Gamma_N \sum_{\sigma, \delta} \epsilon_{\sigma} [f_{\sigma, \delta}^e(\pi_0 + \pi_{\bar{\sigma}}) - f_{\sigma, \delta}^h(\pi_{\sigma} + \pi_{\uparrow\downarrow})], \quad (2a)$$

$$\langle J_q \rangle = \Gamma_N \sum_{\sigma, \delta} e [f_{\sigma, \delta}^e(\pi_0 + \pi_{\bar{\sigma}}) - f_{\sigma, \delta}^h(\pi_{\sigma} + \pi_{\uparrow\downarrow})], \quad (2b)$$

where we denoted $f_{\sigma, \delta}^e = f(\epsilon_{\sigma} + \delta U)$ and $f_{\sigma, \delta}^h = 1 - f(\epsilon_{\sigma} + \delta U)$ the Fermi-Dirac distributions for electrons and holes, respectively, the populations of the density operator, $\pi_0 = \langle 0 | \pi | 0 \rangle$, $\pi_{\sigma} = \langle \sigma | \pi | \sigma \rangle$, $\pi_{\uparrow\downarrow} = \langle \uparrow\downarrow | \pi | \uparrow\downarrow \rangle$, and with $\uparrow\downarrow = \downarrow$. Explicit expressions are provided in Appendix B. Hereafter, we set electron charge $e = 1$, Boltzmann constant $k_B = 1$, and $\hbar = 1$.

Associated with the transport of energy and electrons between the dot and the normal-metal reservoir, we identify the average heat current entering the system, $\dot{Q} := \langle J_E \rangle - \mu_N \langle J_q \rangle$, and the average electrical output power delivered to the normal metal, $\dot{W}_q := -\mu_N \langle J_q \rangle$, as usual [78]. In addition, we identify the average output power extracted into the superconductor from the time-dependent Hamiltonian, $\dot{W}_S := -\text{Tr}[\dot{H}_S(t) \rho_S(t)]$, which in the interaction picture and for the steady-state regime reads

$$\dot{W}_S = i\Gamma_S (2\epsilon + U) (\pi_c - \pi_c^*), \quad (3)$$

where $\pi_c = \langle 0 | \pi | \uparrow\downarrow \rangle$. Notice that this is a coherent work contribution which only depends on the (nonzero) off-diagonal elements of π in the H_d basis, connecting the even-parity QD states by a Cooper pair. The first law in the setup hence reads $\dot{W}_S + \dot{W}_q = \dot{Q}$, ensuring the balance

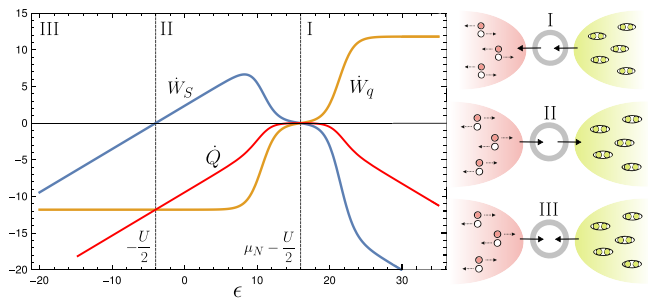


FIG. 2. Three operating regimes for the Andreev reflection engine as characterized by the electric power output at the normal reservoir \dot{W}_q (orange solid-line), the driving power extracted in the superconductor \dot{W}_S (orange solid-line), and the heat absorbed from the reservoir \dot{Q} (red solid-line) as a function of the dot energy level ϵ in $k_B T$ units (left panel) and their corresponding illustrations in terms of the direction of the currents (right panel). Power and heat current values are given in units of $\Gamma_N k_B T$ and we took $U = 8k_B T$, $\mu_N = 20k_B T$, $\Delta_Z = 2k_B T$, and $\Gamma_S = 0.6\Gamma_N$.

between output work in both terminals and input heat from the normal metal [79]

In Fig. 2 we show the three main regimes of operation of the NS hybrid device as a function of the dot level ϵ for fixed values of Coulomb repulsion $U > 0$ and chemical potential $\mu_N > \mu_S = 0$. In regime (I), $\epsilon > \mu_N - U/2$, the electric current enters the normal-metal generating output power \dot{W}_q at the expense of the work exerted by the superconductor, $\dot{W}_S < 0$. Maximum output electric power $\dot{W}_q^{\max} = \mu\Gamma_N[4\Gamma_S^2/(\Gamma_N^2 + 4\Gamma_S^2)]$ is quickly reached as ϵ is increased. On the contrary, if (II) $-U/2 < \epsilon < \mu_N - U/2$, work is extracted in the superconductor through the generation of Cooper pairs $\dot{W}_S > 0$ using an input electrical current from the normal metal acting as a load, $\dot{W}_q < 0$. In this regime, the superconducting power reaches its maximum, but obtaining an analytical expression for it was not possible. Finally, for (III) $\epsilon < -U/2$, $\dot{W}_S < 0$ becomes negative, together with $\dot{W}_q < 0$, and hence power from both superconducting and normal-metal contacts is consumed. In the three regimes, heat is dissipated into the environment $\dot{Q} < 0$ leading to a non-negative entropy production rate:

$$\Sigma = -\dot{Q}/T = -(\dot{W}_S + \dot{W}_q)/T \geq 0. \quad (4)$$

The equilibrium point is achieved precisely in the interface between regimes I and II for $\epsilon = \mu_N - U/2$, where both electrical and superconducting currents change sign leading to zero dissipation. This corresponds to the condition of (global) detailed balance in the setup, obtained from $f_{\uparrow,1}^e f_{\downarrow,1}^e = f_{\uparrow,0}^h f_{\downarrow,0}^h$.

The efficiencies of regimes I and II are obtained by dividing the output power by the corresponding input load as $\eta_I := \dot{W}_q/(-\dot{W}_S)$ and $\eta_{II} := \dot{W}_S/(-\dot{W}_q)$, which lead to remarkably simple expressions:

$$\eta_I = \frac{2\mu_N}{2\epsilon + U} \leq 1, \quad \eta_{II} = \frac{2\epsilon + U}{2\mu_N} \leq 1, \quad (5)$$

where the upper bounds follow from the second law of thermodynamics in the setup, as expressed in Eq. (4). Notice that, contrary to the case of quantum heat engines and

refrigerators, the efficiency of the Andreev reflection engine is not bounded by the Carnot efficiency, but by 1, as it corresponds to work-to-work transducers [46]. Moreover, similar to other models of steady-state engines working in a continuous operation mode, maximum efficiency can only be obtained by approaching the equilibrium point, leading to vanishing power output [45,78,80], and it verifies universal relations constraining maximum power and minimum dissipation in the linear-response regime [47,81,82].

III. ENHANCED STABILITY FROM DEPARTURES IN TUR AND KUR

Beyond the power output and the efficiency of an engine, a third key element for the assessment of its performance is the stability of the output power. Generated power is affected by unavoidable fluctuations induced by environmental noise, and it may spoil its reliability [83–85]. The TUR has a privileged position to capture the core of the tradeoff between power, efficiency, and stability, since it bounds all current fluctuations by dissipation, $\text{var}[X]^2/\langle X \rangle^2 \geq 2k_B/\Sigma$, for any current, e.g., $X = J_E, J_q, \dots$, where $\text{var}[X] = \sqrt{\langle (X - \langle X \rangle)^2 \rangle}$ is the variance or uncertainty of the considered current [49–51]. Indeed, it allows a quantitative characterization of this tradeoff through the so-called normalized constancy [53], which in the present setup reads, for the electric power,

$$\mathcal{C}_T = 2k_B T \frac{\eta_I \mathcal{F}_q}{(1 - \eta_I) \dot{W}_q} \leq 1, \quad (6)$$

where $\mathcal{F}_q := \langle J_q \rangle^2 / \text{var}[J_q]^2$ denotes the electric signal-to-noise ratio (squared inverse relative error) quantifying the reliability of the engine's output current, and we applied the TUR to obtain the right-hand-side inequality. This implies that low efficiency is a price to pay for accessing a large signal-to-noise ratio (and hence a reliable engine) at finite output power. We notice that the TUR strictly bounds the optimal performance of any classical steady-state engine following classical dynamics, as characterized by its power, efficiency, and stability [53]. However, in the Andreev reflection engine, it is possible to achieve enhanced constancy in relevant operating regimes, as its quantum coherent (but Markovian) evolution induced by superconductivity allows the breakdown of the TUR. We explicitly show the TUR departure by obtaining analytical expressions of the current variance $\text{var}[J_q]$ that are used to compute the signal-to-noise ratio \mathcal{F}_q and the normalized constancy \mathcal{C}_T , using the full-counting-statistics formalism [86–89]. In particular, we obtained the generalized quantum master equation including four counting fields accounting for the input-output exchange of electrons in the normal-metal contact. The cumulants are then computed following the inverse counting statistics method formulated in Ref. [89], from which the current variance $\text{var}[J_q]$ is obtained (see Appendix C).

Our results are shown in Fig. 3(c), where we plot \mathcal{C}_T as a function of $\epsilon - \mu_N$ and the Coulomb repulsion U . The classical upper bound $\mathcal{C}_T = 1$ is highlighted by the red dashed line, while yellow (light) tones denote quantum-enhanced constancy. While classical steady-state engines achieve unit constancy only at the equilibrium point (detailed balance

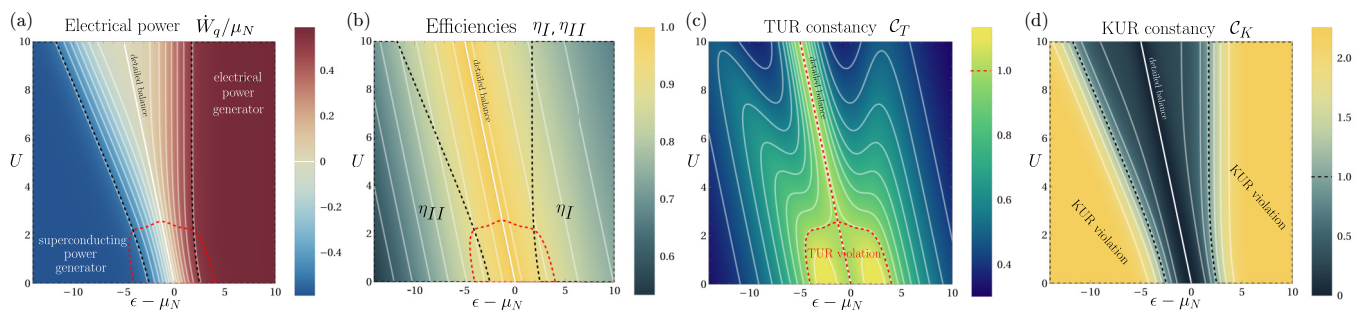


FIG. 3. (a) Electrical output power in $\mu_N\Gamma_N$ units vs $\epsilon - \mu_N$ (dot level height on the top the conductor chemical potential) and U (Coulomb interaction). The global detailed balance condition depicted in white ($\epsilon - \mu_N = -U/2$) separates regimes with electrical power generation (regime I) and superconducting power generator (regime II). (b) Corresponding efficiency for the superconducting work to electrical power conversion (η_I) and for electrical power to superconducting work (η_{II}). (c) TUR constancy in the plane $(\epsilon - \mu_N, U)$ where regions leading to TUR violations $C_T > 1$ are marked by the dashed red line. (d) KUR constancy in the plane $(\epsilon - \mu_N, U)$ and violations $C_K > 1$ marked by dashed black lines. Parameters: $\Gamma_S = 0.6\Gamma_N$, $k_B T = 1$, and $\Delta z = 0$.

line in the figure), our Andreev reflection engine allows a quantum-mechanical enhancement of its thermodynamic performance ($C_T \simeq 1.2$) in regimes of high efficiency $\eta > 0.9$ and near the maximum output power region $\dot{W}_q \simeq (0.4-0.5)\mu_N\Gamma_N$, as can be appreciated in Figs. 3(a) and 3(b), in which the region leading to TUR violations has also been included to guide the eye.

Far from equilibrium, however, dissipation is not the only quantity of interest; time-symmetric quantities may play an important role as well [64]. An important example is dynamical activity (or frenesy) [90–93] characterizing the total volume of transitions in a system per unit time, regardless of the net current directions. In our setup, it reads

$$\mathcal{K} = \Gamma_N \sum_{\sigma, \delta} [f_{\sigma, \delta}^e(\pi_0 + \pi_{\bar{\sigma}}) + f_{\sigma, \delta}^h(\pi_{\sigma} + \pi_{\uparrow\downarrow})]; \quad (7)$$

for the explicit expression, see the Appendix B. It has been shown that dynamical activity also bounds all steady-state currents by means of the KUR, as $\text{var}[X]^2/(X)^2 \geq \mathcal{K}^{-1}$ for $X = J_E, J_q, \dots$, providing a tighter constraint to the noise-to-current ratio than the TUR in far-from-equilibrium conditions [63,66]. The KUR allows us to directly introduce a new normalized constancy bounded by 1 for classical Markov dynamics in nonequilibrium steady states:

$$C_K = \frac{\mathcal{F}_q}{\mathcal{K}} \leq 1, \quad (8)$$

to be compared with the TUR-based normalized constancy in Eq. (6). The above inequality provides a complementary (strict) constraint to the stability of any classical steady-state engine, and it highlights the fact that in order to increase the signal-to-noise ratio, a larger dynamical activity is necessary, independent of the incurred dissipation.

Remarkably, we find that the Andreev engine exhibits large violations of the KUR-normalized constancy (up to $C_K \simeq 2.2$.) in extensive parameter regimes, as shown in Fig. 3(d), as soon as we deviate from equilibrium, i.e., from the centered white line representing detailed balance conditions. The region where Eq. (8) is violated is highlighted in yellow (light), with the classical maximum value represented by the black dotted curves. This region includes parameters for which maximum power has been (almost) saturated, $\dot{W}_q \simeq 0.5\mu_N\Gamma_N$

[see Fig. 3(a), where the region with enhanced KUR-normalized constancy is also plotted], and the engine efficiency starts to decrease with respect to the region showing TUR violations, $\eta_I \simeq 0.9-0.6$ [both regions are also compared in Fig. 3(b)]. Therefore, it turns out that the most accentuated quantum consequences on the engine precision occur indeed in far-from-equilibrium conditions, and they are in general undetected by the TUR. There is, however, a small region where both TUR and KUR are simultaneously violated, where the Andreev reflection engine shows a high output power ($\dot{W}_q \simeq 0.5\mu_N\Gamma_N$) together with a stability not achievable with similar values of efficiency ($\eta_I \simeq 0.9$) by any classical steady-state engine.

IV. EXPERIMENTAL DIRECTIONS AND CLOSING

Hybrid systems benefit from Andreev processes serving as the basis for the construction of Andreev reflection engines operating as work-to-work transducers. Notably, these engines exhibit significant violations of the TUR and the KUR at large efficiencies and maximum power (doubling KUR violations predicted in normal double quantum dots [65]). We propose for its experimental realization a semiconductor nanowire QD as motivated by the recent experimental activity on the subgap transport regime [74–76]. Specifically, a device consisting of a nanowire QD tunnel-coupled to a normal electrode, and partially covered by a layer of a large-gap superconducting material, where our results may be tested from measurements of current fluctuations. [Typical parameters: $\Delta = 2.5$ meV (niobium) [30,94] or $\Delta \sim 0.55$ (vanadium with Ti and Al), $U \approx 0.2$ meV, $T \in [0.1, 1$ K] [74], and tunneling $\Gamma_N \in [1, 5$ $\mu\text{eV}]$ as in experiments in the weakly coupled regime [95,96].] Out of the large-gap regime we expect that quasiparticle transport will weaken the violation of TUR and KUR. Coherent assisted devices such as the Andreev reflection engine presented here, showing large departures from the classical TUR and KUR bounds, open the door to construct highly stable and efficient quantum machines under low-dissipation conditions. On the other hand, the ultimate precision bounds achievable in hybrid normal-superconducting quantum conductors remain an open question for future research [97].

ACKNOWLEDGMENTS

G.M. acknowledges funding from Spanish MICINN through the ‘‘Ram3n y Cajal’’ (RYC2021-031121-I) and ‘‘Juan de la Cierva’’ programs (IJC2019-039592-I). R.L. acknowledges the financial support by Grant No. PDR2020/12 sponsored by the Comunitat Aut3noma de les Illes Balears through the Direcci3n General de Pol3tica Universitaria i Recerca with funds from the Tourist Stay Tax Law ITS 2017-006, Grants No. PID2020-117347GB-I00, and No. LINKB20072 from the CSIC i-link program 2021. This work has been partially supported by the Mar3a de Maeztu project CEX2021-001164-M funded by the MCIN/AEI/10.13039/501100011033.

APPENDIX A: MASTER EQUATION DERIVATION

The Hamiltonian of the QD system interacting with normal and superconducting leads reads

$$\begin{aligned} \mathcal{H} = & \sum_{\sigma} \left[\epsilon_{\sigma} d_{\sigma}^{\dagger} d_{\sigma} + \frac{U}{2} d_{\sigma}^{\dagger} d_{\sigma} d_{\bar{\sigma}}^{\dagger} d_{\bar{\sigma}} \right] \\ & + \sum_{\sigma} \sum_{k_{\alpha}} V_{k_{\alpha}} (c_{k_{\alpha}}^{\dagger} d_{\sigma} + \text{H.c.}) + \sum_{k_N} \epsilon_{k_N} c_{k_N}^{\dagger} c_{k_N} \\ & + \sum_{k_S} \epsilon_{k_S} c_{k_S}^{\dagger} c_{k_S} + \Delta (c_{k_S}^{\dagger} c_{k_S}^{\dagger} + \text{H.c.}). \end{aligned} \quad (\text{A1})$$

As in the main text, $\epsilon_{\uparrow,\downarrow} = \epsilon \pm \Delta_Z$ is the energy level for the dot, and U is the Coulomb repulsion. Electrons are annihilated in the dot by the operator d_{σ} with spin denoted by $\sigma = \{\uparrow, \downarrow\}$ ($\bar{\sigma}$ denotes the opposite spin to σ). Here k_{α} is the wave vector for the electronic states in the superconducting and metallic reservoirs, $\alpha = \{S, N\}$. Δ denotes the superconducting gap. Operators c_{k_N} and c_{k_S} represent the destruction operator for electrons at the normal (N) and superconducting (S) electrodes. The tunneling amplitudes between the normal-to-dot and superconducting-to-dot parts are denoted by $V_N \equiv V_{k_N}$ and $V_S \equiv V_{k_S}$, respectively, which are considered independent of k . The relevant QD states are denoted for short as $|\uparrow\rangle$, $|\downarrow\rangle$ for one electron on the dot with respective spin, $|0\rangle$ for no electrons, and $|\uparrow\downarrow\rangle$, corresponding to a Cooper pair in the QD.

From Eq. (A1) we perform two approaches: (i) the on-site Coulomb interaction is considered weak enough to allow a mean-field treatment, and (ii) we follow Ref. [72] and we adopt an effective Hamiltonian description corresponding to the large-gap limit (subgap transport $\Delta \gg \Gamma_N, k_B T$) by taking $\Delta \rightarrow \infty$. In that case, the continuum part of the charge current due to the quasiparticle contribution is negligible [43,73–76]. Under these considerations, the QD is ‘‘proximitized’’ by the superconductivity introducing an effective local pairing term

denoted by Γ_S . Consequently, the QD Hamiltonian is composed of a bare term $H_d = \sum_{\sigma} \epsilon_{\sigma} d_{\sigma}^{\dagger} d_{\sigma} + U d_{\uparrow}^{\dagger} d_{\uparrow} d_{\downarrow}^{\dagger} d_{\downarrow}$ and the pairing term $H_S(t) = \Gamma_S (d_{\uparrow}^{\dagger} d_{\downarrow}^{\dagger} e^{i(2\epsilon+U)t} + d_{\downarrow} d_{\uparrow} e^{-i(2\epsilon+U)t})$, whereas the superconducting electrode is traced out.

In the weak-coupling limit of the QD normal-metal interaction, and under Born-Markov approximations ($V_N^2 \ll \max\{|\epsilon_{\sigma} - \mu_N|, k_B T\}$ [77]), the driven-dissipative dynamics of the system can be described by means of a quantum master equation [98,99]. Moreover, in the limit of weak interaction with the superconductor, one can treat $H_S(t)$ as a perturbation to the bare QD Hamiltonian H_d , and perform the secular approximation up to leading order [100] to obtain a master equation in Gorini-Kossakovsky-Sudarshan-Lindblad (GKSL) or simply Lindblad form:

$$\begin{aligned} \dot{\rho}_S(t) = & -i[H_d + H_S(t) + H_{LS}, \rho_S(t)] \\ & + \sum_k \mathcal{D}_k[\rho_S(t)] + O(V_N^2 \Gamma_S), \end{aligned} \quad (\text{A2})$$

which remains valid as long as $O(V_N^2 \Gamma_S) \sim O(V_N^3)$ or greater. Here H_{LS} is the so-called Lamb-shift Hamiltonian, and we obtain dissipators $\mathcal{D}_k[\rho] = L_k \rho L_k^{\dagger} - \frac{1}{2} \{L_k^{\dagger} L_k \rho\}$ (with $k = \{\sigma, \delta\}$) for the set of Lindblad operators $L_{\sigma,\delta}^+ = \sqrt{\Gamma_N f(\epsilon_{\sigma} + \delta U)} d_{\sigma}^{\dagger}$ and $L_{\sigma,\delta}^- = \sqrt{\Gamma_N [1 - f(\epsilon_{\sigma} + \delta U)]} d_{\sigma}$, with $\delta = \{0, 1\}$. They produce jumps between the bare H_d QD states, with $f(E) = 1/[1 + \exp[\beta(E - \mu)]]$ the Fermi-Dirac distribution function [$\beta = (k_B T)^{-1}$, where k_B is the Boltzmann constant and T is the temperature] and $\Gamma_N = \pi V_N^2 \nu_N$ is considered as a constant (ν_N is the DOS at the normal contact).

The terms H_{LS} and $\mathcal{D}_k[\rho_S(t)]$ above are of the order V_N^2 , while further terms of order $O(V_N^2 \Gamma_S)$ are neglected, justifying that the presence of the superconductor driving term $H_S(t)$ does not alter the dissipative interaction between the QD and the normal metal [99]. This procedure is standard for obtaining a local master equation [100], while alternative ways have been discussed, e.g., in Refs. [101–104]. Moreover, as is customary in open quantum systems, we neglect the Lamb-shift Hamiltonian H_{LS} since it only leads to a (small) renormalization of the original energies [98,99]. Taking these considerations into account, and shifting to the rotating frame with respect to H_d , we recover, from Eq. (A2), the master equation (1).

From the master equation (1) we can obtain the Pauli equations for the QD level occupations $p_i := \langle i|\rho|i\rangle$ for $i = \{0, \uparrow, \downarrow, \uparrow\downarrow\}$ and the only relevant off-diagonal term $c := \langle 0|\rho|\uparrow\downarrow\rangle$ induced by the superconductor coherent driving. Below we display the Pauli equations in matrix form as $d\vec{p}(t)/dt = W\vec{p}(t)$ with column vector $\vec{p} = (p_0, p_{\uparrow}, p_{\downarrow}, p_{\uparrow\downarrow}, c, c^*)^T$ and rate matrix W :

$$\begin{pmatrix} \dot{p}_0 \\ \dot{p}_{\downarrow} \\ \dot{p}_{\uparrow} \\ \dot{p}_{\uparrow\downarrow} \\ \dot{c} \\ \dot{c}^* \end{pmatrix} = \begin{pmatrix} -(k_{\uparrow}^+ + k_{\downarrow}^+) & k_{\downarrow}^- & k_{\uparrow}^- & 0 & i\Gamma_S & -i\Gamma_S \\ k_{\downarrow}^+ & -(k_{\downarrow}^- + r_{\uparrow}^+) & 0 & r_{\uparrow}^- & 0 & 0 \\ k_{\uparrow}^+ & 0 & -(k_{\uparrow}^- + r_{\downarrow}^+) & r_{\downarrow}^- & 0 & 0 \\ 0 & r_{\uparrow}^+ & r_{\downarrow}^+ & -(r_{\uparrow}^- + r_{\downarrow}^-) & -i\Gamma_S & i\Gamma_S \\ i\Gamma_S & 0 & 0 & -i\Gamma_S & -\Gamma & 0 \\ -i\Gamma_S & 0 & 0 & i\Gamma_S & 0 & -\Gamma \end{pmatrix} \begin{pmatrix} p_0 \\ p_{\downarrow} \\ p_{\uparrow} \\ p_{\uparrow\downarrow} \\ c \\ c^* \end{pmatrix}, \quad (\text{A3})$$

where i is the pure imaginary complex unit, and the transition rates that appear in the rate matrix W read $k_\sigma^\pm := \Gamma_N f(\epsilon_\sigma)$ and $r_\sigma^\pm := \Gamma_N f(\epsilon_{d\sigma} + U)$. Moreover, for ease of notation, we used $\Gamma := \sum_\sigma (k_\sigma^+ + r_\sigma^-)/2$. Notice that the transition rates k_σ^\pm and r_σ^\pm stand for adding an electron on the dot (+) with spin σ and for subtraction of an electron (-) with spin σ , and we distinguished the cases in which the quantum dot is either empty (k -rates) or singly occupied (r -rates).

APPENDIX B: MAIN THERMODYNAMIC QUANTITIES

In this Appendix, we provide some of the analytical expressions for the main quantities characterizing the performance of the Andreev reflection engine introduced in the main text. First, we provide expressions for the energy and charge currents in Eqs. (2a) and (2b):

$$\langle J_E \rangle = \frac{4\Gamma_N(2\epsilon + U)\Gamma_S^2(f_{\uparrow,1}^e f_{\downarrow,1}^e - f_{\uparrow,0}^h f_{\downarrow,0}^h)}{\sum_\sigma (f_{\sigma,1}^e + f_{\sigma,0}^h)(4\Gamma_S^2 + \Gamma_N^2[1 - \prod_\sigma (f_{\sigma,1}^e - f_{\sigma,0}^h)])}, \quad (\text{B1})$$

$$\langle J_q \rangle = \frac{4\Gamma_N\Gamma_S^2(f_{\uparrow,1}^e f_{\downarrow,1}^e - f_{\uparrow,0}^h f_{\downarrow,0}^h)}{\sum_\sigma (f_{\sigma,1}^e + f_{\sigma,0}^h)(4\Gamma_S^2 + \Gamma_N^2[1 - \prod_\sigma (f_{\sigma,1}^e - f_{\sigma,0}^h)])}, \quad (\text{B2})$$

from which we can easily check that $\langle J_E \rangle = (2\epsilon + U)\langle J_q \rangle$, and that the detailed balance condition $f_{\uparrow,1}^e f_{\downarrow,1}^e = f_{\uparrow,0}^h f_{\downarrow,0}^h$ leads immediately to $\langle J_E \rangle = \langle J_q \rangle = 0$. On the other hand, the average output power in the superconductor from Eq. (3)

reads

$$\dot{W}_S = \frac{4\Gamma_N(2\epsilon + U)\Gamma_S^2(f_{\uparrow,1}^e f_{\downarrow,1}^e - f_{\uparrow,0}^h f_{\downarrow,0}^h)}{\sum_\sigma (f_{\sigma,1}^e + f_{\sigma,0}^h)(4\Gamma_S^2 + \Gamma_N^2[1 - \prod_\sigma (f_{\sigma,1}^e - f_{\sigma,0}^h)])}, \quad (\text{B3})$$

hence verifying $\dot{W}_S = \langle J_E \rangle$, as pointed out in the main text. The entropy production in Eq. (4) is then given by

$$\Sigma = \frac{4\Gamma_N(2\mu - 2\epsilon - U)\Gamma_S^2(f_{\uparrow,1}^e f_{\downarrow,1}^e - f_{\uparrow,0}^h f_{\downarrow,0}^h)}{T \sum_\sigma (f_{\sigma,1}^e + f_{\sigma,0}^h)(4\Gamma_S^2 + \Gamma_N^2[1 - \prod_\sigma (f_{\sigma,1}^e - f_{\sigma,0}^h)])}, \quad (\text{B4})$$

and the dynamical activity in Eq. (7) reads

$$\mathcal{K} = \Gamma_N \left[\frac{\Gamma_N^2(K_1 + K_2) \sum_\sigma (f_{\sigma,1}^e + f_{\sigma,0}^h)}{\sum_\sigma (f_{\sigma,1}^e + f_{\sigma,0}^h)(4\Gamma_S^2 + \Gamma_N^2[1 - \prod_\sigma (f_{\sigma,1}^e - f_{\sigma,0}^h)])} - \frac{4\Gamma_S^2 K_3 (f_{\downarrow,1}^e + f_{\uparrow,0}^h)}{\sum_\sigma (f_{\sigma,1}^e + f_{\sigma,0}^h)(4\Gamma_S^2 + \Gamma_N^2[1 - \prod_\sigma (f_{\sigma,1}^e - f_{\sigma,0}^h)])} \right]. \quad (\text{B5})$$

Finally, the electric power signal-to-noise ratio appearing in TUR and KUR expressions [Eqs. (6) and (8)] is given by

$$\mathcal{F}_q = \frac{(f_{\uparrow,1}^e f_{\downarrow,1}^e - f_{\uparrow,0}^h f_{\downarrow,0}^h) \sum_\sigma (f_{\sigma,1}^e + f_{\sigma,0}^h)}{2\mu[F_1 + F_2 + F_3 + F_4]}. \quad (\text{B6})$$

In the above expressions for the dynamical activity and electric signal-to-noise ratio, we have introduced the following functions to simplify the expressions:

$$\begin{aligned} K_1 &= (f_{\downarrow,0}^e)^2 \left(f_{\uparrow,1}^e f_{\downarrow,1}^e + f_{\uparrow,0}^e \sum_\sigma f_{\sigma,1}^h - f_{\uparrow,1}^h - 1 \right) + f_{\uparrow,0}^e \left(2f_{\uparrow,0}^h - f_{\downarrow,1}^e \left[(f_{\uparrow,1}^e)^2 + f_{\uparrow,1}^e f_{\downarrow,1}^e - \sum_\sigma f_{\sigma,1}^h - f_{\uparrow,0}^e (f_{\uparrow,1}^e + 1) \right] \right), \\ K_2 &= f_{\downarrow,0}^e \left(2 + (f_{\uparrow,0}^e)^2 \sum_\sigma f_{\sigma,1}^h - f_{\uparrow,0}^e \left[(f_{\downarrow,1}^e)^2 + f_{\uparrow,1}^e f_{\downarrow,1}^e - \sum_\sigma f_{\sigma,1}^h \right] \right) + f_{\uparrow,0}^e \left[(f_{\downarrow,1}^e)^2 + (f_{\uparrow,1}^e)^2 + 4(f_{\uparrow,1}^e f_{\downarrow,1}^e - 1) - \sum_\sigma f_{\sigma,1}^e \right], \\ K_3 &= (f_{\downarrow,0}^e)^2 + (f_{\uparrow,1}^e + 1)(f_{\uparrow,1}^h + f_{\downarrow,1}^h + f_{\uparrow,0}^h) + f_{\downarrow,0}^e (2f_{\uparrow,1}^e - f_{\downarrow,0}^e - f_{\downarrow,1}^h), \\ F_1 &= \sum_\sigma (f_{\sigma,1}^e + f_{\sigma,0}^h)^2 [f_{\uparrow,1}^e f_{\downarrow,1}^e - f_{\downarrow,0}^e - f_{\uparrow,1}^e f_{\downarrow,0}^e (1 + f_{\downarrow,1}^e) + f_{\uparrow,0}^e f_{\downarrow,0}^e (f_{\uparrow,1}^e - f_{\downarrow,1}^e) - f_{\uparrow,0}^e (f_{\uparrow,1}^e f_{\downarrow,1}^e - f_{\downarrow,1}^h)], \\ F_2 &= 4\Gamma_S^2 \frac{(f_{\uparrow,1}^e f_{\downarrow,1}^e - f_{\uparrow,0}^h f_{\downarrow,0}^h) [8 + (f_{\downarrow,0}^e)^2 - (f_{\downarrow,1}^e)^2 + f_{\uparrow,0}^e (f_{\uparrow,0}^e - 8) + f_{\downarrow,0}^e (6f_{\uparrow,0}^e - 8) - 6f_{\uparrow,1}^e f_{\downarrow,1}^e - (f_{\uparrow,1}^e)^2]}{4\Gamma_S^2 + \Gamma_N^2 [1 - \prod_\sigma (f_{\sigma,1}^e - f_{\sigma,0}^h)]}, \\ F_3 &= 4\Gamma_S^2 \left(\frac{f_{\uparrow,1}^e f_{\downarrow,1}^e - f_{\uparrow,0}^h f_{\downarrow,0}^h}{4\Gamma_S^2 + \Gamma_N^2 [1 - \prod_\sigma (f_{\sigma,1}^e - f_{\sigma,0}^h)]} \right)^2, \\ F_4 &= 4\Gamma_S^2 \left[10 - \sum_\sigma (f_{\sigma,1}^e - f_{\sigma,0}^h) \right] + \left[18 + 5 \sum_\sigma (f_{\sigma,1}^e - f_{\sigma,0}^h) + (f_{\downarrow,0}^e)^2 [f_{\uparrow,0}^e - f_{\uparrow,1}^e] + f_{\downarrow,1}^e (f_{\uparrow,0}^e - f_{\uparrow,1}^e) \right. \\ &\quad \left. \times [10 + f_{\downarrow,1}^e - f_{\uparrow,0}^e + f_{\uparrow,1}^e] + f_{\downarrow,0}^e [(f_{\uparrow,0}^e)^2 + 2f_{\uparrow,1}^e (5 + f_{\downarrow,1}^e) + (f_{\uparrow,1}^e)^2 - 2f_{\uparrow,0}^e (5 + f_{\uparrow,1}^e + f_{\downarrow,1}^e)] \right]. \quad (\text{B7}) \end{aligned}$$

APPENDIX C: FULL COUNTING STATISTICS

To calculate the variance of the currents in the QD systems and test TUR and KUR expressions, we employ the full counting statistics (FCS) formalism [15,87–89]. A generalized quantum master equation can be obtained by including counting fields for the electron transport within dissipative terms:

$$\dot{\rho}_G(t, \chi_\uparrow, \chi_\downarrow) = -i\Gamma_S[d_\uparrow^\dagger d_\downarrow^\dagger + d_\uparrow d_\downarrow, \rho_G(t, \chi_\uparrow, \chi_\downarrow)] + \sum_k \bar{D}_k[\rho_G(t, \chi_\uparrow, \chi_\downarrow)], \tag{C1}$$

where $\rho_G(t, 0, 0) = \rho(t)$, and we introduced modified dissipators (again $k = \{\sigma, \delta\}$):

$$\bar{D}_k[\rho_G] = L_k \rho_G L_k^\dagger e^{-i\chi_\sigma} - \frac{1}{2} \{L_k^\dagger L_k \rho_G\}. \tag{C2}$$

The variables χ_\uparrow and χ_\downarrow represent the counting fields for \uparrow and \downarrow electrons exchanged with the normal metal, respectively, associated with projective measurements of the number of particles in the normal metal. The solution of the generalized master equation above provides direct information on the generating function for particle exchange statistics with the reservoir with different spins, N_\uparrow and N_\downarrow , as $\text{Tr}[\rho_G(t, \chi_\uparrow, \chi_\downarrow)] = G(\chi_\uparrow, \chi_\downarrow, t) = \int dN_\uparrow dN_\downarrow P(N_\uparrow, N_\downarrow) e^{i(\chi_\uparrow N_\uparrow + \chi_\downarrow N_\downarrow)}$.

As for the case of the original master equation, the counting-field-dependent generalized master equation can be linearized and written in matrix form as $d\bar{p}_G(t)/dt = W_G(\chi_\uparrow, \chi_\downarrow)\bar{p}_G(t)$ with

$$W_G(\chi_\uparrow, \chi_\downarrow) = \begin{pmatrix} -(k_\uparrow^+ + k_\downarrow^+) & k_\downarrow^- \exp(-i\chi_\downarrow) & k_\uparrow^- \exp(-i\chi_\uparrow) & 0 & i\Gamma_S & -i\Gamma_S \\ k_\downarrow^+ \exp(i\chi_\downarrow) & -(k_\downarrow^- + r_\uparrow^+) & 0 & r_\uparrow^- \exp(-i\chi_\uparrow) & 0 & 0 \\ k_\uparrow^+ \exp(i\chi_\uparrow) & 0 & -(k_\downarrow^- + r_\uparrow^+) & r_\downarrow^- \exp(-i\chi_\downarrow) & 0 & 0 \\ 0 & r_\uparrow^+ \exp(i\chi_\uparrow) & r_\downarrow^+ \exp(i\chi_\downarrow) & -(r_\uparrow^- + r_\downarrow^-) & -i\Gamma_S & i\Gamma_S \\ i\Gamma_S & 0 & 0 & -i\Gamma_S & -\Gamma & 0 \\ -i\Gamma_S & 0 & 0 & i\Gamma_S & 0 & -\Gamma \end{pmatrix}, \tag{C3}$$

to be compared with the rate matrix W in Eq. (A3) above. The cumulants are computed following the inverse counting statistics method formulated in Ref. [89]. In this method, the characteristic polynomial of matrix W_G , namely $P(\lambda) := -\det[W_G(\chi_\uparrow, \chi_\downarrow) - \lambda\mathbb{1}]$, is written as a series in terms of powers of its eigenvalues,

$$P(\lambda) = \sum_{\mu=0}^M a_\mu \lambda^\mu = \lambda^M + a_{M-1} \lambda^{M-1} + \sum_{\mu}^{M-2} \sum_{j=0}^{\infty} \sum_{l=0}^{\infty} a_\mu^{(j,l)} \frac{\chi_\uparrow^j \chi_\downarrow^l}{j! l!} \lambda^\mu, \tag{C4}$$

with $M = 6$ the dimension of W_G , and where in the second line the coefficients $a_\mu(\chi_\uparrow, \chi_\downarrow)$ have been expanded in a (two-variable) Taylor series around the vicinity of $(\chi_\uparrow = 0, \chi_\downarrow = 0)$. Above we used the short-hand notation $a_\mu^{(j,l)} := \partial_{\chi_\uparrow}^j \partial_{\chi_\downarrow}^l a_\mu|_{(\chi_\uparrow, \chi_\downarrow)=0}$ and $a_\mu^{(0)} = a_\mu|_{(\chi_\uparrow, \chi_\downarrow)=0}$. Following Ref. [89], the derivatives of the polynomial coefficients with respect to the counting fields can be identified with the different cumulants of the electron currents. Therefore, by knowing the series coefficients of the characteristic polynomial, the different cumulants can be obtained in a systematic way.

The characteristic polynomial $P(\lambda)$ can be analytically obtained from W_G in Eq. (C3), from which the relevant coefficients can be calculated as

$$a_0 = P(\lambda = 0), \quad a_1 = \left. \frac{\partial P(\lambda)}{\partial \lambda} \right|_{\lambda=0}, \quad a_2 = \left. \frac{1}{2} \frac{\partial^2 P(\lambda)}{\partial \lambda^2} \right|_{\lambda=0}. \tag{C5}$$

As a second step, we calculated their derivatives with respect to the counting fields:

$$a_0^{(j,l)} = (-i)^{j+l} \left. \frac{\partial^{j+l} a_0}{\partial \chi_\uparrow^j \partial \chi_\downarrow^l} \right|_{(\chi_\uparrow, \chi_\downarrow)=0},$$

$$a_{1,\sigma}^{(j,l)} = (-i)^{j+l} \left. \frac{\partial^{j+l} a_1}{\partial \chi_\uparrow^j \partial \chi_\downarrow^l} \right|_{(\chi_\uparrow, \chi_\downarrow)=0},$$

$$a_{2,\sigma}^{(j,l)} = (-i)^{j+l} \left. \frac{\partial^{j+l} a_2}{\partial \chi_\uparrow^j \partial \chi_\downarrow^l} \right|_{(\chi_\uparrow, \chi_\downarrow)=0}. \tag{C6}$$

Finally, from the coefficients above, we obtain the first and second cumulants of the spin charge currents, namely the average currents for spin $\sigma = \uparrow, \downarrow$, their corresponding variances, and the covariance between the two currents:

$$\langle J_q^{(\uparrow)} \rangle = -\frac{a_0^{(1,0)}}{a_1^{(0)}}, \quad \langle J_q^{(\downarrow)} \rangle = -\frac{a_0^{(0,1)}}{a_1^{(0)}}, \tag{C7}$$

$$\text{var}[J_q^{(\uparrow)}] = -\frac{a_0^{(2,0)} + 2a_0^{(1,0)} J_q^{(\uparrow)} + 2a_2^{(0)} J_q^{(\uparrow)2}}{a_1^{(0)}}, \tag{C8}$$

$$\text{var}[J_q^{(\downarrow)}] = -\frac{a_0^{(0,2)} + 2a_0^{(0,1)} J_q^{(\downarrow)} + 2a_2^{(0)} J_q^{(\downarrow)2}}{a_1^{(0)}}, \tag{C9}$$

$$\text{covar}[J_q^{(\uparrow)}, J_q^{(\downarrow)}] = -\frac{a_0^{(1,1)} + a_1^{(1,0)} J_q^{(\uparrow)} + a_0^{(0,1)} J_q^{(\downarrow)}}{a_1^{(0)}} + \frac{a_2^{(0)} (J_q^{(\uparrow)2} + J_q^{(\downarrow)2})}{a_1^{(0)}}. \tag{C10}$$

We emphasize that the obtained expressions for the average charge current $\langle J_q \rangle = \sum_\sigma \langle J_q^{(\sigma)} \rangle$ coincide with the expression

given in Eq. (2b). Moreover, we point out a typo in the expression of the second cumulant c_2 in Eq. (11) of Ref. [89], where a'_0 should read $a''_0 \neq a'_0$, and we corrected it in the above

$$\text{var}[W_q] = \mu_N^2(\text{var}[J_q^{(\uparrow)}] + \text{var}[J_q^{(\downarrow)}]) + 2 \text{covar}[J_q^{(\uparrow)}, J_q^{(\downarrow)}] = 4\mu_N^2 \text{var}[J_q^{(\sigma)}], \quad (\text{C11})$$

where the last equality follows from the fact that the symmetry of our system leads to $\text{var}[J_q^{(\uparrow)}] = \text{var}[J_q^{(\downarrow)}] =$

expressions. From the variance of the electron currents with spins, $\sigma = \{\uparrow, \downarrow\}$, we can obtain the variance of the electrical power output as

$\text{covar}[J_q^{(\uparrow)}, J_q^{(\downarrow)}]$. These expressions have been used to calculate the electric power signal-to-noise ratio given in Eq. (B6).

- [1] A. F. Andreev, The thermal conductivity of the intermediate state in superconductors, *Sov. Phys.-JETP* **19**, 1228 (1964).
- [2] A. Martín-Rodero and A. L. Yeyati, Josephson and Andreev transport through quantum dots, *Adv. Phys.* **60**, 899 (2011).
- [3] S. De Franceschi, L. Kouwenhoven, C. Schönberger, and W. Wernsdorfer, Hybrid superconductor–quantum dot devices, *Nat. Nanotechnol.* **5**, 703 (2010).
- [4] P. Jarillo-Herrero, J. A. van Dam, and L. P. Kouwenhoven, Quantum supercurrent transistors in carbon nanotubes, *Nature (London)* **439**, 953 (2006).
- [5] H. I. Jørgensen, T. Novotný, K. Grove-Rasmussen, K. Flensberg, and P. E. Lindelof, Critical current $0-\pi$ transition in designed Josephson quantum dot junctions, *Nano Lett.* **7**, 2441 (2007).
- [6] M. Lee, R. López, H. Q. Xu, and G. Platero, Proposal for detection of the $0'$ and π' phases in quantum-dot Josephson junctions, *Phys. Rev. Lett.* **129**, 207701 (2022).
- [7] J. S. Lim and R. López, Subgap spectrum for an interacting hybrid superconducting quantum dot, *Phys. Rev. B* **101**, 245427 (2020).
- [8] M. R. Buitelaar, W. Belzig, T. Nussbaumer, B. Babić, C. Bruder, and C. Schönberger, Multiple andreev reflections in a carbon nanotube quantum dot, *Phys. Rev. Lett.* **91**, 057005 (2003).
- [9] J. J. A. Baselmans, A. F. Morpurgo, B. J. V. Wees, and T. M. Klapwijk, Reversing the direction of the supercurrent in a controllable Josephson junction, *Nature (London)* **397**, 43 (1999).
- [10] J. Huang, F. Pierre, T. T. Heikkilä, F. K. Wilhelm, and N. O. Birge, Observation of a controllable π -junction in a 3-terminal Josephson device, *Phys. Rev. B* **66**, 020507(R) (2002).
- [11] J. A. van Dam, Y. V. Nazarov, E. P. A. M. Bakkers, S. De Franceschi, and L. P. Kouwenhoven, Supercurrent reversal in quantum dots, *Nature (London)* **442**, 667 (2006).
- [12] M.-S. Choi, C. Bruder, and D. Loss, Spin-dependent Josephson current through double quantum dots and measurement of entangled electron states, *Phys. Rev. B* **62**, 13569 (2000).
- [13] P. Recher, E. V. Sukhorukov, and D. Loss, Andreev tunneling, coulomb blockade, and resonant transport of nonlocal spin-entangled electrons, *Phys. Rev. B* **63**, 165314 (2001).
- [14] P. Samuelsson, E. V. Sukhorukov, and M. Büttiker, Electrical current noise of a beamsplitter as a test of spin entanglement, *Phys. Rev. B* **70**, 115330 (2004).
- [15] G. B. Lesovik, T. Martin, and G. Blatter, Electronic entanglement in the vicinity of a superconductor, *Eur. Phys. J. B* **24**, 287 (2001).
- [16] O. Sauret, D. Feinberg, and T. Martin, Quantum master equations for the superconductor-quantum dot entangler, *Phys. Rev. B* **70**, 245313 (2004).
- [17] L. Hofstetter, S. Csonka, J. Nygård, and C. Schönberger, Cooper pair splitter realized in a two-quantum-dot y-junction, *Nature (London)* **461**, 960 (2009).
- [18] L. G. Herrmann, F. Portier, P. Roche, A. L. Yeyati, T. Kontos, and C. Strunk, Carbon nanotubes as cooper-pair beam splitters, *Phys. Rev. Lett.* **104**, 026801 (2010).
- [19] G. Wang, T. Dvir, G. P. Mazur, C.-X. Liu, N. van Loo, S. L. D. ten Haaf, A. Bordin, S. Gazibegovic, G. Badawy, E. P. A. M. Bakkers, M. Wimmer, and L. P. Kouwenhoven, Singlet and triplet cooper pair splitting in hybrid superconducting nanowires, *Nature (London)* **612**, 448 (2022).
- [20] H. le Sueur, P. Joyez, H. Pothier, C. Urbina, and D. Esteve, Phase controlled superconducting proximity effect probed by tunneling spectroscopy, *Phys. Rev. Lett.* **100**, 197002 (2008).
- [21] V. T. Petrashov, V. N. Antonov, P. Delsing, and T. Claeson, Phase controlled conductance of mesoscopic structures with superconducting “mirrors”, *Phys. Rev. Lett.* **74**, 5268 (1995).
- [22] A. Dimoulas, J. P. Heida, B. J. V. Wees, T. M. Klapwijk, W. V. D. Graaf, and G. Borghs, Phase-dependent resistance in a superconductor-two-dimensional-electron-gas quasiparticle interferometer, *Phys. Rev. Lett.* **74**, 602 (1995).
- [23] H. Pothier, S. Guéron, D. Esteve, and M. H. Devoret, Flux-modulated Andreev current caused by electronic interference, *Phys. Rev. Lett.* **73**, 2488 (1994).
- [24] J. Clarke, A. N. Cleland, M. H. Devoret, D. Esteve, and J. M. Martinis, Quantum mechanics of a macroscopic variable: The phase difference of a Josephson junction, *Science* **239**, 992 (1988).
- [25] P. Spathis, S. Biswas, S. Roddaro, L. Sorba, F. Giazotto, and F. Beltram, Hybrid InAs nanowire–vanadium proximity SQUID, *Nanotechnology* **22**, 105201 (2011).
- [26] C. M. Natarajan, M. G. Tanner, and R. H. Hadfield, Superconducting nanowire single-photon detectors: Physics and applications, *Supercond. Sci. Technol.* **25**, 063001 (2012).
- [27] M. H. Devoret and R. J. Schoelkopf, Superconducting circuits for quantum information: An outlook, *Science* **339**, 1169 (2013).
- [28] G. de Lange, B. van Heck, A. Bruno, D. J. van Woerkom, A. Geresdi, S. R. Plissard, E. P. A. M. Bakkers, A. R. Akhmerov, and L. DiCarlo, Realization of microwave quantum circuits using hybrid superconducting-semiconducting nanowire Josephson elements, *Phys. Rev. Lett.* **115**, 127002 (2015).
- [29] M. Hays, V. Fatemi, D. Bouman, J. Cerrillo, S. Diamond, K. Serniak, T. Connolly, P. Krogstrup, J. Nygård, A. L. Yeyati, A. Geresdi, and M. H. Devoret, Coherent manipulation of an Andreev spin qubit, *Science* **373**, 430 (2021).

- [30] V. Mourik, K. Zuo, S. M. Frolov, S. R. Plissard, E. P. A. M. Bakkers, and L. P. Kouwenhoven, Signatures of Majorana fermions in hybrid superconductor-semiconductor nanowire devices, *Science* **336**, 1003 (2012).
- [31] M. T. Deng, S. Vaitiekėnas, E. B. Hansen, J. Danon, M. Leijnse, K. Flensberg, J. Nygård, P. Krogstrup, and C. M. Marcus, Majorana bound state in a coupled quantum-dot hybrid-nanowire system, *Science* **354**, 1557 (2016).
- [32] D. Aasen, M. Hell, R. V. Mishmash, A. Higginbotham, J. Danon, M. Leijnse, T. S. Jespersen, J. A. Folk, C. M. Marcus, K. Flensberg, and J. Alicea, Milestones toward Majorana-based quantum computing, *Phys. Rev. X* **6**, 031016 (2016).
- [33] S.-Y. Hwang, R. López, and D. Sánchez, Large thermoelectric power and figure of merit in a ferromagnetic-quantum dot-superconducting device, *Phys. Rev. B* **94**, 054506 (2016).
- [34] M. M. Leivo, J. P. Pekola, and D. V. Averin, Efficient peltier refrigeration by a pair of normal metal/insulator/superconductor junctions, *Appl. Phys. Lett.* **68**, 1996 (1996).
- [35] J. P. Pekola, T. T. Heikkilä, A. M. Savin, J. T. Flyktman, F. Giazotto, and F. W. J. Hekking, Limitations in cooling electrons using normal-metal-superconductor tunnel junctions, *Phys. Rev. Lett.* **92**, 056804 (2004).
- [36] A. Fornieri, M. J. Martínez-Pérez, and F. Giazotto, A normal metal tunnel-junction heat diode, *Appl. Phys. Lett.* **104**, 183108 (2014).
- [37] R. Sánchez, Correlation-induced refrigeration with superconducting single-electron transistors, *Appl. Phys. Lett.* **111**, 223103 (2017).
- [38] A. Fornieri and F. Giazotto, Towards phase-coherent caloritronics in superconducting circuits, *Nat. Nanotechnol.* **12**, 944 (2017).
- [39] J. Mastomäki, S. Roddaro, M. Rocci, V. Zannier, D. Ercolani, L. Sorba, I. J. Maasilta, N. Ligato, A. Fornieri, E. Strambini, and F. Giazotto, InAs nanowire superconducting tunnel junctions: Quasiparticle spectroscopy, thermometry, and nanorefrigeration, *Nano Res.* **10**, 3468 (2017).
- [40] R. Sánchez, P. Buset, and A. L. Yeyati, Cooling by cooper pair splitting, *Phys. Rev. B* **98**, 241414(R) (2018).
- [41] R. Sánchez, P. Samuelsson, and P. P. Potts, Autonomous conversion of information to work in quantum dots, *Phys. Rev. Res.* **1**, 033066 (2019).
- [42] M. Acciai, F. Hajiloo, F. Hassler, and J. Splettstoesser, Phase-coherent heat circulators with normal or superconducting contacts, *Phys. Rev. B* **103**, 085409 (2021).
- [43] S. M. Tabatabaei, D. Sánchez, A. L. Yeyati, and R. Sánchez, Nonlocal quantum heat engines made of hybrid superconducting devices, *Phys. Rev. B* **106**, 115419 (2022).
- [44] G. Blasi, F. Giazotto, and G. Haack, Hybrid normal-superconducting Aharonov-Bohm quantum thermal device, *Quantum Sci. Technol.* **8**, 015023 (2023).
- [45] R. Kosloff and A. Levy, Quantum heat engines and refrigerators: Continuous devices, *Annu. Rev. Phys. Chem.* **65**, 365 (2014).
- [46] U. Seifert, Efficiency of autonomous soft nanomachines at maximum power, *Phys. Rev. Lett.* **106**, 020601 (2011).
- [47] K. Proesmans, Y. Dreher, M. C. V. Gavrilov, J. Bechhoefer, and C. Van den Broeck, Brownian duet: A novel tale of thermodynamic efficiency, *Phys. Rev. X* **6**, 041010 (2016).
- [48] M. Carrega, M. Sasseti, and U. Weiss, Optimal work-to-work conversion of a nonlinear quantum Brownian duet, *Phys. Rev. A* **99**, 062111 (2019).
- [49] A. C. Barato and U. Seifert, Thermodynamic uncertainty relation for biomolecular processes, *Phys. Rev. Lett.* **114**, 158101 (2015).
- [50] T. R. Gingrich, J. M. Horowitz, N. Perunov, and J. L. England, Dissipation bounds all steady-state fluctuations, *Phys. Rev. Lett.* **116**, 120601 (2016).
- [51] J. M. Horowitz and T. R. Gingrich, Thermodynamic uncertainty relations constrain non-equilibrium fluctuations, *Nat. Phys.* **16**, 15 (2020).
- [52] U. Seifert, From stochastic thermodynamics to thermodynamic inference, *Annu. Rev. Condens. Matter Phys.* **10**, 171 (2019).
- [53] P. Pietzonka and U. Seifert, Universal trade-off between power, efficiency, and constancy in steady-state heat engines, *Phys. Rev. Lett.* **120**, 190602 (2018).
- [54] K. Brandner, T. Hanazato, and K. Saito, Thermodynamic bounds on precision in ballistic multiterminal transport, *Phys. Rev. Lett.* **120**, 090601 (2018).
- [55] B. K. Agarwalla and D. Segal, Assessing the validity of the thermodynamic uncertainty relation in quantum systems, *Phys. Rev. B* **98**, 155438 (2018).
- [56] E. Potanina, C. Flindt, M. Moskalets, and K. Brandner, Thermodynamic bounds on coherent transport in periodically driven conductors, *Phys. Rev. X* **11**, 021013 (2021).
- [57] K. Ptaszyński, Coherence-enhanced constancy of a quantum thermoelectric generator, *Phys. Rev. B* **98**, 085425 (2018).
- [58] J. Liu and D. Segal, Thermodynamic uncertainty relation in quantum thermoelectric junctions, *Phys. Rev. E* **99**, 062141 (2019).
- [59] L. M. Cangemi, V. Cataudella, G. Benenti, M. Sasseti, and G. De Filippis, Violation of thermodynamics uncertainty relations in a periodically driven work-to-work converter from weak to strong dissipation, *Phys. Rev. B* **102**, 165418 (2020).
- [60] A. A. S. Kalae, A. Wacker, and P. P. Potts, Violating the thermodynamic uncertainty relation in the three-level maser, *Phys. Rev. E* **104**, L012103 (2021).
- [61] A. Rignon-Bret, G. Guarnieri, J. Goold, and M. T. Mitchison, Thermodynamics of precision in quantum nanomachines, *Phys. Rev. E* **103**, 012133 (2021).
- [62] L. d. S. Souza, G. Manzano, R. Fazio, and F. Iemini, Collective effects on the performance and stability of quantum heat engines, *Phys. Rev. E* **106**, 014143 (2022).
- [63] I. D. Terlizzi and M. Baiesi, Kinetic uncertainty relation, *J. Phys. A* **52**, 02LT03 (2019).
- [64] C. Maes, *Non-Dissipative Effects in Nonequilibrium Systems* (Springer, New York, 2018).
- [65] K. Prech, P. Johansson, E. Nyholm, G. T. Landi, C. Verdozzi, P. Samuelsson, and P. P. Potts, Entanglement and thermokinetic uncertainty relations in coherent mesoscopic transport, *Phys. Rev. Res.* **5**, 023155 (2023).
- [66] K. Hiura and S.-i. Sasa, Kinetic uncertainty relation on first-passage time for accumulated current, *Phys. Rev. E* **103**, L050103 (2021).
- [67] V. T. Vo, T. V. Vu, and Y. Hasegawa, Unified thermodynamic-kinetic uncertainty relation, *J. Phys. A* **55**, 405004 (2022).
- [68] G. Guarnieri, G. T. Landi, S. R. Clark, and J. Goold, Thermodynamics of precision in quantum

- nonequilibrium steady states, *Phys. Rev. Res.* **1**, 033021 (2019).
- [69] F. Carollo, R. L. Jack, and J. P. Garrahan, Unraveling the large deviation statistics of Markovian open quantum systems, *Phys. Rev. Lett.* **122**, 130605 (2019).
- [70] Y. Hasegawa, Thermodynamic uncertainty relation for general open quantum systems, *Phys. Rev. Lett.* **126**, 010602 (2021).
- [71] T. Van Vu and K. Saito, Thermodynamics of precision in Markovian open quantum dynamics, *Phys. Rev. Lett.* **128**, 140602 (2022).
- [72] A. V. Rozhkov and D. P. Arovas, Interacting-impurity Josephson junction: Variational wave functions and Slave-Boson mean-field theory, *Phys. Rev. B* **62**, 6687 (2000).
- [73] S. M. Tabatabaei, D. Sánchez, A. L. Yeyati, and R. Sánchez, Andreev-Coulomb drag in coupled quantum dots, *Phys. Rev. Lett.* **125**, 247701 (2020).
- [74] E. J. H. Lee, X. Jiang, M. Houzet, R. Aguado, C. M. Lieber, and S. De Franceschi, Spin-resolved Andreev levels and parity crossings in hybrid superconductor–semiconductor nanostructures, *Nat. Nanotechnol.* **9**, 79 (2014).
- [75] E. J. H. Lee, X. Jiang, R. Žitko, R. Aguado, C. M. Lieber, and S. De Franceschi, Scaling of subgap excitations in a superconductor-semiconductor nanowire quantum dot, *Phys. Rev. B* **95**, 180502(R) (2017).
- [76] A. Bargerbos, M. Pita-Vidal, R. Žitko, L. J. Splitthoff, L. Grünhaupt, J. J. Wesdorp, Y. Liu, L. P. Kouwenhoven, R. Aguado, C. K. Andersen, A. Kou, and B. van Heck, Spectroscopy of spin-split Andreev levels in a quantum dot with superconducting leads, [arXiv:2208.09314](https://arxiv.org/abs/2208.09314) [cond-mat.mes-hall].
- [77] P. P. Potts, A. A. S. Kalaei, and A. Wacker, A thermodynamically consistent Markovian master equation beyond the secular approximation, *New J. Phys.* **23**, 123013 (2021).
- [78] G. Benenti, G. Casati, K. Saito, and R. S. Whitney, Fundamental aspects of steady-state conversion of heat to work at the nanoscale, *Phys. Rep.* **694**, 1 (2017).
- [79] Furthermore, one can verify that any output work on the superconducting contact comes from an energy current from the normal-metal, $\dot{W}_S = \langle J_E \rangle$, as expected.
- [80] N. Shiraishi, K. Saito, and H. Tasaki, Universal trade-off relation between power and efficiency for heat engines, *Phys. Rev. Lett.* **117**, 190601 (2016).
- [81] K. Proesmans, B. Cleuren, and C. Van den Broeck, Power-efficiency-dissipation relations in linear thermodynamics, *Phys. Rev. Lett.* **116**, 220601 (2016).
- [82] S. Saryal, M. Gerry, I. Khait, D. Segal, and B. K. Agarwalla, Universal bounds on fluctuations in continuous thermal machines, *Phys. Rev. Lett.* **127**, 190603 (2021).
- [83] V. Holubec and A. Ryabov, Cycling tames power fluctuations near optimum efficiency, *Phys. Rev. Lett.* **121**, 120601 (2018).
- [84] S. Kheradsoud, N. Dashti, M. Misiorny, P. P. Potts, J. Splettstoesser, and P. Samuelsson, Power, efficiency and fluctuations in a quantum point contact as steady-state thermoelectric heat engine, *Entropy* **21**, 777 (2019).
- [85] H. J. D. Miller, M. H. Mohammady, M. Perarnau-Llobet, and G. Guarnieri, Thermodynamic uncertainty relation in slowly driven quantum heat engines, *Phys. Rev. Lett.* **126**, 210603 (2021).
- [86] L. S. Levitov, H. Lee, and G. B. Lesovik, Electron counting statistics and coherent states of electric current, *J. Math. Phys.* **37**, 4845 (1996).
- [87] Y. Nazarov and M. Kindermann, Full counting statistics of a general quantum mechanical variable, *Eur. Phys. J. B* **35**, 413 (2003).
- [88] M. Esposito and G. Schaller, Stochastic thermodynamics for “Maxwell demon” feedbacks, *Europhys. Lett.* **99**, 30003 (2012).
- [89] M. Bruderer, L. D. Contreras-Pulido, M. Thaller, L. Sironi, D. Obreschkow, and M. B. Plenio, Inverse counting statistics for stochastic and open quantum systems: The characteristic polynomial approach, *New J. Phys.* **16**, 033030 (2014).
- [90] E. Roldán and P. Vivo, Exact distributions of currents and frenesy for Markov bridges, *Phys. Rev. E* **100**, 042108 (2019).
- [91] O. Bénichou, P. Illien, G. Oshanin, A. Sarracino, and R. Voituriez, Microscopic theory for negative differential mobility in crowded environments, *Phys. Rev. Lett.* **113**, 268002 (2014).
- [92] J. P. Garrahan, R. L. Jack, V. Lecomte, E. Pitard, K. van Duijvendijk, and F. van Wijland, Dynamical first-order phase transition in kinetically constrained models of glasses, *Phys. Rev. Lett.* **98**, 195702 (2007).
- [93] G. Volpe, I. Buttinoni, D. Vogt, H.-J. Kümmerer, and C. Bechinger, Microswimmers in patterned environments, *Soft Matter* **7**, 8810 (2011).
- [94] M. Deng, C. Yu, G. Huang, M. Larsson, P. Caroff, and H. Xu, Anomalous zero-bias conductance peak in a Nb–InSb nanowire–Nb hybrid device, *Nano Lett.* **12**, 6414 (2012).
- [95] E. B. Foxman, P. L. McEuen, U. Meirav, N. S. Wingreen, Y. Meir, P. A. Belk, N. R. Belk, M. A. Kastner, and S. J. Wind, Effects of quantum levels on transport through a Coulomb island, *Phys. Rev. B* **47**, 10020 (1993).
- [96] G. Jaliel, R. K. Puddy, R. Sánchez, A. N. Jordan, B. Sothmann, I. Farrer, J. P. Griffiths, D. A. Ritchie, and C. G. Smith, Experimental realization of a quantum dot energy harvester, *Phys. Rev. Lett.* **123**, 117701 (2019).
- [97] A. M. Timpanaro, G. Guarnieri, and G. T. Landi, The most precise quantum thermoelectric, [arXiv:2106.10205](https://arxiv.org/abs/2106.10205) [quant-ph].
- [98] H.-P. Breuer and F. Petruccione, *The Theory of Open Quantum Systems* (Oxford University Press, Oxford, 2002).
- [99] H. Wiseman and G. J. Milburn, *Quantum Measurement and Control* (Cambridge University Press, Cambridge, 2010).
- [100] A. S. Trushechkin and I. V. Volovich, Perturbative treatment of inter-site couplings in the local description of open quantum networks, *Europhys. Lett.* **113**, 30005 (2016).
- [101] P. P. Hofer, M. Perarnau-Llobet, L. D. M. Miranda, G. Haack, R. Silva, J. B. Brask, and N. Brunner, Markovian master equations for quantum thermal machines: Local versus global approach, *New J. Phys.* **19**, 123037 (2017).
- [102] F. Barra, The thermodynamic cost of driving quantum systems by their boundaries, *Sci. Rep.* **5**, 14873 (2015).
- [103] G. De Chiara, G. Landi, A. Hewgill, B. Reid, A. Ferraro, A. Roncaglia, and M. Antezza, Reconciliation of quantum local master equations with thermodynamics, *New J. Phys.* **20**, 113024 (2018).
- [104] M. Cattaneo, G. Giorgi, S. Maniscalco, and R. Zambrini, Local versus global master equation with common and separate baths: superiority of the global approach in partial secular approximation, *New J. Phys.* **21**, 113045 (2019).